RSC Advances

PAPER

View Article Online
View Journal | View Issue

Cite this: *RSC Adv.*, 2021, **11**, 17346

A new family of decanuclear Ln_7Cr_3 clusters exhibiting a magnetocaloric effect†

Jia-Jia Yin,‡[a] Tian-Qi Lu,‡[a] Cheng Chen,[a] Hai-Yan Shi,[b] Gui-Lin Zhuang,[c] Jun Zheng,[a] Xiaolong Fang[d] and Xiu-Ying Zheng*[ab]

Two dimeric Ln–Cr clusters with formula $\{Ln(H_2O)_8[Ln_6Cr_3(L)_6(CH_3COO)_6(\mu_3\text{-}OH)_{12}(H_2O)_{12}]\}\cdot(ClO_4)_6\cdot xH_2O$ (Ln = **Gd**, x = 35 for **1** and Ln = **Dy**, x = 45 for **2**, HL = 2-pyrazinecarboxylic acid) were obtained by a ligand-controlled hydrolytic method with a mixed ligand system (2-pyrazinecarboxylic acid and acetate). Single crystal structure analysis showed that two trigonal bipyramids of $[Gd_3Cr_2(\mu_3\text{-}OH)_6]^{9+}$ worked as building blocks in constructing the metal-oxo cluster core of $[Gd_6Cr_3(\mu_3\text{-}OH)_{12}]^{15+}$ by sharing a common top – a Cr^{3+} ion. Additionally, compound **1** forms a three-dimensional framework with a one-dimensional nanopore channel along the *a*-axis through a hydrogen-bond interaction between the cationic cluster core and the free mononuclear cation $[Gd(H_2O)_8]^{3+}$ and the π-bond interactions of the pyrazine groups on the two cationic cluster cores. Magnetic calculations indicated a weak ferromagnetic coupling interaction for Gd···Gd and Gd···Cr in compound **1**, with its magnetic entropy change ($-\Delta S_m$) reaching 21.1 J kg^{-1} K^{-1} at 5 K, 7 T, while compound **2** displayed an obvious frequency-dependency at H_{dc} = 2000 Oe.

Received 8th April 2021
Accepted 5th May 2021

DOI: 10.1039/d1ra02734d

rsc.li/rsc-advances

1. Introduction

Due to its existence for many years, the chemistry of lanthanide-transition metal clusters is no longer an emerging discipline, but researchers' enthusiasm for high-nuclearity lanthanide-transition metal clusters is still unabated. Specifically, researchers focused initially on their beautiful and nearly perfect molecular structures (such as Keplerate-type $Ln_{20}Ni_{30}$,[1] nesting doll-like $Ln_{54}Ni_{54}$ [2] and $Ln_{60}Ni_{76}$),[3,4] later on exploration and promotion of their properties in optics,[5,6] magnetism[7–11] and catalysis,[12–15] and recently on their assembly mechanism.[16–19] These reports indicate that high-nuclearity lanthanide-transition metal clusters are still an interesting research field for further investigation.

Compared with other frequently reported mature lanthanide-transition metal clusters,[20] there are relatively few reports on lanthanide–chromium (Ln–Cr) clusters, especially those with more than ten metals.[21–28] The combination of Cr^{3+} ions of negative magnetic anisotropy and a large spin ground state value with Ln^{3+} ions can form Ln–Cr polymetallic complexes with good magnetic properties, such as single molecule magnet (SMM)[29–32] and magnetocaloric effect (MCE).[27,33–36] Cryogenic magnetic refrigerant depends on MCE to achieve the cooling purpose in the low temperature zone. High-nuclearity Ln–Cr clusters have a potential application value as cryogenic magnetic cooling materials due to the advantages of a large spin ground state value, high magnetic density, and negative magnetic anisotropy. However, the inert nature of Cr^{3+} ions makes it difficult to combine with Ln^{3+} ions, suggesting the necessity of a suitable ligand or synthetic strategy for constructing high-nuclearity Ln–Cr clusters. Additionally, MCE is closely related with magnetic coupling between metal ions.[36,37] The magnetic exchange interaction is slightly stronger between 3d–4f metal ions than between 4f–4f metal ions, which can avoid the strong magnetic exchange interaction between 3d–3d metal ions. Thus far, few studies have been performed regarding the magnetic exchange between metal ions in high-nuclearity Ln–Cr clusters.[22,26,27]

Ligand-controlled hydrolysis is shown as an effective strategy for synthesizing high-nuclearity lanthanide-containing metal clusters,[38,39] due to the hydrolysis control of metal ions by ligands, and their protection and stabilization of the metal core. Hard–Soft Acid–Base (HSAB) theory reveals the chelating ligand

[a]*Institutes of Physical Science and Information Technology, Key Laboratory of Structure and Functional Regulation of Hybrid Materials of Ministry of Education, Photoelectric Conversion Energy Materials and Devices Key Laboratory of Anhui Province, Anhui University, Hefei, 230601, China. E-mail: xyzheng@ahu.edu.cn*

[b]*State Key Laboratory of Physical Chemistry of Solid Surfaces, Department of Chemistry, College of Chemistry and Chemical Engineering, Xiamen University, Xiamen, 361005, China*

[c]*College of Chemical Engineering, Zhejiang University of Technology, Hangzhou, 310032, China*

[d]*College of Materials and Chemical Engineering, Anhui Jianzhu University, Hefei, 230601, China*

† Electronic supplementary information (ESI) available: IR, TGA, Fig. S1–S8 and Tables S1–S4. CCDC 1964545 and 1964546. For ESI and crystallographic data in CIF or other electronic format see DOI: 10.1039/d1ra02734d

‡ These authors contributed equally to this work.

containing N and O groups as the first candidate for synthesizing high-nuclearity lanthanide-transition metal clusters. Here, we selected 2-pyrazinecarboxylic acid as the primary ligand and acetate as co-ligand to control the degree of hydrolysis of metal ions, and obtained two dimeric Ln–Cr clusters with the formulas $\{Ln(H_2O)_8[Ln_6Cr_3(L)_6(CH_3COO)_6(\mu_3\text{-}OH)_{12}(H_2O)_{12}]\}\cdot(ClO_4)_6\cdot xH_2O$ (Ln = **Gd**, $x = 35$ for **1** and Ln = **Dy**, $x = 45$ for **2**, HL = 2-pyrazinecarboxylic acid). Single crystal structure analysis showed the formation of the metal core $\{Ln_6Cr_3\}$ from two trigonal bipyramids $\{Ln_3Cr_2\}$ sharing a common top of Cr^{3+} ion. Magnetic calculations indicated a weak ferromagnetic coupling interaction for Gd···Gd and Gd···Cr in compound **1**, with its magnetic entropy change ($-\Delta S_m$) reaching 21.1 J kg^{-1} K^{-1} at 5 K, 7 T, while compound **2** displayed an obvious frequency-dependency at $H_{dc} = 2000$ Oe.

2. Experimental section

2.1 Materials and methods

In this study, all commercially purchased reagents were of analytical grade and used as purchased without further purification. Ln_2O_3 (Ln = Gd/Dy) was dissolved by slowly adding perchloric acid aqueous solution (70.0–72.0%, 64.0 mL) which was performed in the fume cupboard. Aqueous solution of $Ln(ClO_4)_3$ (1.0 M) was obtained by diluting the concentrated solution to 250 mL (pH ~ 0.25). The magnetic susceptibility data (2–300 K) of powder samples were obtained with a SQUID magnetometer (Quantum Design MPMSXL). A Vario EL-3 elemental analyzer was used for elemental analysis (EA) of C, H, and N in the powder samples after drying for one week in an air dryer, and a NICOLET iS50 FT-IR spectrophotometer with pressed KBr pellets was used to record the infrared spectra. Meanwhile, a NETZSCH TG209F3 thermal analyzer was used for thermogravimetric analysis (TGA) at a heating rate of 2.0 °C min^{-1} and an air flow of 20.0 L min^{-1}. The purity of the products was checked by X-ray powder diffraction on a BRUKER D2 PHASER powder X-ray diffractometer. The powder samples used here were obtained by milling the hexagonal flake crystals. UV-Vis absorption spectra was performed by TU1810 DPC ultraviolet spectrograph.

2.2 Synthesis of $\{Gd(H_2O)_8[Gd_6Cr_3(L)_6(CH_3COO)_6(\mu_3\text{-}OH)_{12}(H_2O)_{12}]\}\cdot(ClO_4)_6\cdot 35H_2O$ (1)

Briefly, $Gd(ClO_4)_3$ (4.0 mmol, 4.0 mL, 1.0 M), $Cr(OAc)_3$ (0.5 mmol, 114.5 mg) and 2-pyrazinecarboxylic acid (HL, 1.0 mmol, 124.1 mg) were dissolved in the round-bottom flask with EtOH (10.0 mL), followed by adjusting pH to about 5.5 with Et_3N (1.5 mmol, 0.2 mL), and then heating and stirring through the reflux condenser tube at 90 °C for 2 h. After filtration, the mixture was placed in a breaker and evaporated in air for 3 days, and then light purple hexagonal flake crystals were collected; yield ~15% based on $Gd(ClO_4)_3$. Anal. calcd (%) for $C_{42}H_{158}N_{12}Cl_6Cr_3Gd_7O_{115}$: C, 12.19; H, 3.96; N, 3.74. Found (%): C, 12.15; H, 3.89; N, 3.80. IR (KBr, cm^{-1}): 3400 (s), 2361 (w), 2341 (w), 2021 (w), 1625 (m), 1587 (m), 1524 (w), 1528 (w), 1474 (w), 1430 (s), 1381 (s), 1347 (m), 1290 (s), 1144 (w), 1110 (w), 1089 (w), 1033 (s), 939 (s), 862 (w), 790 (m), 736 (w), 721 (w), 676 (m), 636 (w), 626 (s), 549 (m), 455 (m).

2.3 Synthesis of $\{Dy(H_2O)_8[Dy_6Cr_3(L)_6(CH_3COO)_6(\mu_3\text{-}OH)_{12}(H_2O)_{12}]\}\cdot(ClO_4)_6\cdot 45H_2O$ (2)

The synthesis was performed using a procedure similar to that for **1** but with $Dy(ClO_4)_3$ (4.0 mmol, 4.0 mL, 1.0 M) to replace $Gd(ClO_4)_3$ (4.0 mmol, 4.0 mL, 1.0 M). After 3 days of air evaporation, light purple hexagonal flake crystals were obtained. (Yield ~ 15%) anal. calcd (%) for $C_{42}H_{178}N_{12}Cl_6Cr_3Dy_7O_{125}$: C, 11.51; H, 3.70; N, 3.56. Found (%): C, 11.55; H, 3.65; N, 3.60. IR (KBr, cm^{-1}): 3400 (s), 2361 (w), 2341 (w), 2021 (w), 1625 (m), 1587 (m), 1524 (w), 1528 (w), 1474 (w), 1430 (s), 1381 (s), 1347 (m), 1290 (s), 1144 (w), 1110 (w), 1089 (w), 1033 (s), 939 (s), 862 (w), 790 (m), 736 (w), 721 (w), 676 (m), 636 (w), 626 (s), 549 (m), 455 (m).

2.4 X-ray crystal structure analysis

A STOE STADIVARI detector was used to collect the crystal X-ray diffraction data of compounds **1–2** with Cu K_α radiation (λ = 1.54184 Å) at 120 K, with the multi-scan program STOE LANA being applied for their absorption corrections, and the Olex2 program for the solution of the structures by the direct method and the anisotropical refinement of non-hydrogen atoms by full-matrix least-squares on F^2.[40–43] The H atoms of the organic ligand were positioned geometrically with C–H = 0.96 Å. The crystal data and the detailed information about the collection and refinement of the complexes are presented in Table S1,† and the selected bonds are shown in Tables S2 and S3.† Charge balance, EA and TGA analyses revealed 6 ClO_4^- and 35 guest water molecules in compound **1** while 6 ClO_4^- and 45 guest water molecules in compound **2**, which were all removed using SQUEEZE due to disorder.[44] In this paper, CCDC contains the ESI crystallographic data submitted to the Cambridge Crystallographic Data Centre with the deposition number of 1964545 and 1964546 for **1–2**, respectively.†

3. Results and discussion

3.1 Synthesis strategy and crystal structure analysis

Ligand-controlled hydrolysis is an effective strategy for synthesis of high-nuclearity metal clusters, and small ligands are the first choice due to their small steric hindrance effect. For high-nuclearity lanthanide-transition metal clusters, the results may be surprising for the hydrolysis of metal ions controlled by the mixed ligands containing both N and O groups and small carboxylic ligands. **Ln_7Cr_3** was prepared through the reaction of HL, $Cr(OAc)_3$ and $Ln(ClO_4)_3$ (Ln = Gd/Dy) with a ratio of 0.5 : 0.5 : 2. Meanwhile, the yield of the products was increased when the molar ratio was changed to 1 : 0.5 : 4. However, **Ln_7Cr_3** could not be obtained by substituting $Cr(OAc)_3$ with $Cr(NO_3)_3\cdot 9H_2O$ in the same procedure, suggesting that acetate plays an important role as co-ligand in the formation of **Ln_7Cr_3**.

Compounds **1** and **2** are isomorphic and crystalize in the monoclinic space group *C*2/*c*, and thus the structure of compound **1** is used as a representative example for detailed

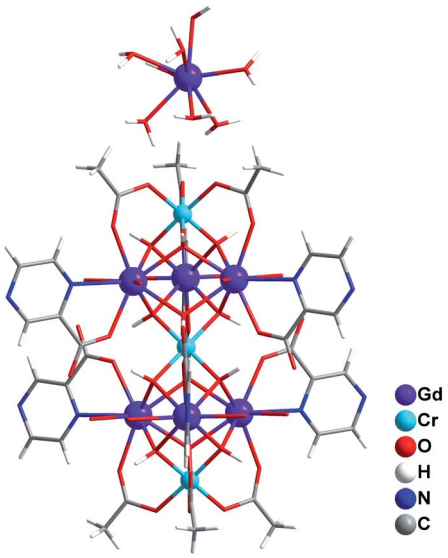

Fig. 1 Ball and stick views of the cationic cluster of $\{Gd(H_2O)_8[Gd_6Cr_3(L)_6(CH_3COO)_6(\mu_3\text{-}OH)_{12}(H_2O)_{12}]\}^{6+}$.

description (Fig. 1). Compound **1** consists of a cationic cluster core of $[Gd_6Cr_3(L)_6(CH_3COO)_6(\mu_3\text{-}OH)_{12}(H_2O)_{12}]^{3+}$, a free mononuclear cation of $[Gd(H_2O)_8]^{3+}$, 6 ClO_4^- anions and 35 guest water molecules. Two cationic cluster units of $[Gd_3Cr_2(L)_3(CH_3COO)_3(\mu_3\text{-}OH)_6]^{3+}$ (Fig. 2a) featuring a trigonal bipyramid configuration share a common vertex of the central Cr^{3+} ion and generate the dimeric cationic cluster core of $[Gd_6Cr_3(L)_6(CH_3COO)_6(\mu_3\text{-}OH)_{12}]^{3+}$ (Fig. 2b). Interestingly, each ligand L^- in **1** is only coordinated with one Gd^{3+} ion by one O atom on the carboxyl and one neighboring N group (Fig. S1†), and the two N groups contained therein are not chelated with any Cr^{3+} ion. For the trigonal bipyramid unit of $[Gd_3Cr_2(L)_3(CH_3COO)_3(\mu_3\text{-}OH)_6(H_2O)_6]^{3+}$, Gd^{3+} and Cr^{3+} ions are linked by one acetate and two μ_3-OH groups, and three Gd^{3+} ions lie in the same plane and are connected to each other through three μ_3-OH groups. Building block strategy is commonly used in metal–organic frameworks.[45] However, investigations on high-nuclearity lanthanide-containing clusters found that theirs structures are usually assembled by simple building blocks,[46] with tetrahedron and tetrapyramid as common basic building blocks in high-nuclearity lanthanide-transition metal clusters, while trigonal bipyramid as building block is rarely reported.[47–49] For compound **1**, the two trigonal bipyramids of $[Gd_3Cr_2(\mu_3\text{-}OH)_6]^{9+}$ (Fig. 2c) can be regarded as the building blocks for constructing the metal-oxo cluster core of $[Gd_6Cr_3(\mu_3\text{-}OH)_{12}]^{15+}$ (Fig. 2d). The three Gd^{3+} ions in the trigonal bipyramid $\{Ln_3Cr_2\}$ (Fig. 2e) are located in the same plane, with the upper and lower metal core units of $\{Ln_3Cr_2\}$ sharing the vertices in a centrally symmetrical manner to produce the metal core of $\{Ln_6Cr_3\}$ (Fig. 2f). The typical trigonal bipyramid (TBP) geometry for the metal core of $\{Ln_3Cr_2\}$ was further confirmed by the structural index parameter $\tau = 0.01$ ($\alpha = 104.3$ and $\beta = 103.7°$) obtained from the equation $\tau = (\beta - \alpha)/60$ reported by Addison *et al.*[50] The distances of Gd···Gd and Gd···Cr are in the range of 3.9962–4.0102 Å and 3.4630–3.5209 Å, respectively, which agree with the previous report.[27] Additionally, compound **1** forms a three-dimensional framework with one-dimensional nanopore channel along the *a*-axis (Fig. 3) through the

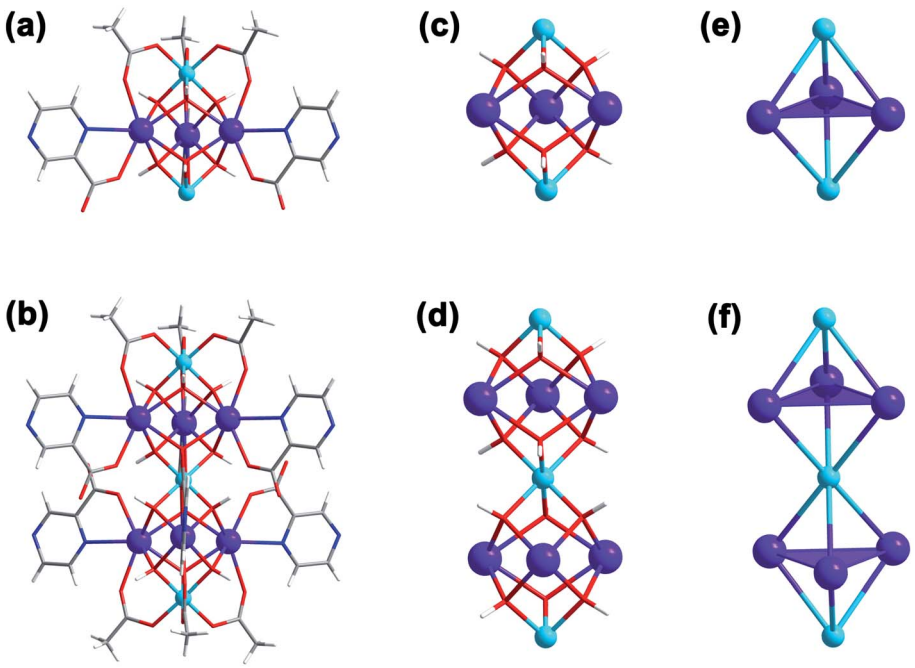

Fig. 2 (a) The cationic cluster unit of $[Gd_3Cr_2(L)_3(CH_3COO)_3(\mu_3\text{-}OH)_6]^{3+}$. (b) The dimeric cationic cluster core of $[Gd_6Cr_3(L)_6(CH_3COO)_6(\mu_3\text{-}OH)_{12}]^{3+}$. (c) Trigonal bipyramid of $[Gd_3Cr_2(\mu_3\text{-}OH)_6]^{9+}$ as the basic building block. (d) The metal-oxo cluster core of $[Gd_6Cr_3(\mu_3\text{-}OH)_{12}]^{15+}$. (e) and (f) The metal arrangement of $\{Ln_3Cr_2\}$ and $\{Ln_6Cr_3\}$, respectively.

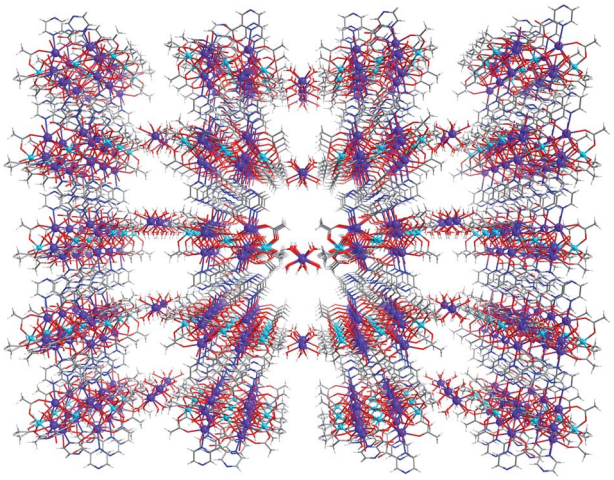

Fig. 3 The three-dimensional framework with one-dimensional nanopore channel along the *a*-axis of compound **1**.

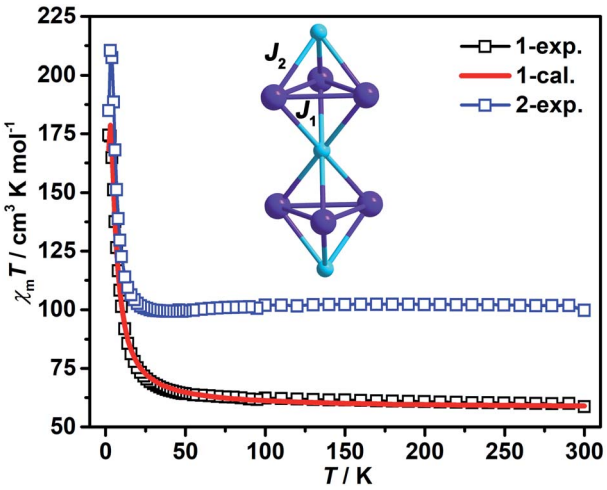

Fig. 4 The magnetic susceptibility of **1–2** was measured using the dried powder samples in the temperature range of 2–300 K and in a magnetic field of 1000 Oe. Experimental values are shown by the point plots and the fitting results by the red line. Insert shows the interaction diagram between metal ions and 2 *J* models.

hydrogen-bond interaction of coordinated water molecules between the cationic cluster core of $[Gd_6Cr_3(L)_6(CH_3COO)_6(\mu_3\text{-}OH)_{12}(H_2O)_{12}]^{3+}$ and the free mononuclear cation of $[Gd(H_2O)_8]^{3+}$ (Fig. S2a†) and the π-bond interactions of the pyrazine groups on the two cationic cluster cores (Fig. S2b†). The guest water molecules play a role in filling the nanopore channel in the framework. In addition, UV-Vis absorption spectra of HL and compounds **1–2** indicates that the main peak at 270 nm belongs to the conjugated transition of the ligand pyrazine ring π–π*.

All of the Cr^{3+} ions are in the hexa-coordinate mode with an octahedral configuration (Fig. S3a†). There are two coordination environments for Gd^{3+} ions in compound **1**. Six Gd^{3+} ions of the cationic cluster core of $[Gd_6Cr_3(L)_6(CH_3COO)_6(\mu_3\text{-}OH)_{12}(H_2O)_{12}]^{3+}$ are in the nona-coordinate mode with a capped square antiprism geometry (Fig. S3b†),[51] and the Gd^{3+} ion from the free mononuclear cation of $[Gd(H_2O)_8]^{3+}$ is in the octa-coordinate mode with a biaugmented trigonal prism geometry (Fig. S3c†).[52] The geometrical configurations of Gd^{3+} ions are further proved by the continuous shape measurement values (CShM) calculated by using the SHAPE program of Alvarez.20 (Table S4†).[53] The bond distances of Gd···O and Cr···O are 2.3371–2.4778 Å and 1.9479–2.0131 Å, respectively, which are similar to the previously reported values for Ln–Cr clusters.[27]

3.2 Magnetic properties

The magnetic susceptibility was measured for compounds **1–2** with the dried powder samples in the temperature range of 2–300 K and in a magnetic field of 1000 Oe (Fig. 4). The $\chi_M T$ values for **1** and **2** at 300 K were found to be 58.7 and 99.8 cm^3 K mol^{-1}, respectively, close to the theoretical values of 60.8 and 104.8 cm^3 K mol^{-1} based on isolated spin centers containing 3 Cr^{3+} ($S = 3/2$, $g = 2$) and 7 Ln^{3+} (Gd^{3+}: $J = 7/2$, $g = 2$, Dy^{3+}: $J = 15/2$, $g = 4/3$) ions. As temperature decreased, the $\chi_M T$ values remained almost unchanged until 100 K, followed by a gradual increase in the temperature range of 100 K and 10 K and then a sharp increase to the maximum of 174.5 and 184.9 cm^3 K mol^{-1} at 2 K for **1** and **2**, respectively, which might be attributed to weak ferromagnetic coupling interaction in the low temperature range. After fitting the $\chi_M T$ *vs.* *T* curves by Curie–Weiss law (Fig. S4a†), compounds **1** and **2** showed the Weiss constant $\theta = 4.05$ and 0.40 K and Curie constant $C = 59.2$ and 100.9 cm^3 K mol^{-1}, respectively. The positive Weiss constant values (4.05 and 1.99 K) displayed the dominance of weak ferromagnetic coupling interaction in **1–2**.

The magnetic coupling interaction in compound **1** was further investigated by using the Quantum Monte Carlo (QMC) method to calculate the magnetic exchange constant *J* between metal ions by fitting the $\chi_M T$ *vs.* *T* curve. As shown in Fig. 4, there are two magnetic coupling paths in **1**, which are labeled as J_1 and J_2, with J_1 for interaction between 2 Gd^{3+} ions in the distance range of 3.9962–4.0101 Å linked by 2 μ_3-OH groups, while J_2 for mixed magnetic interaction between 1 μ_2-OAc and 2 μ_3-OH bridges for Gd···Cr in the distance range of 3.5029–3.5523 Å. The optimal calculated results are $J_1 = 0.367$ cm^{-1}, $J_2 = 0.431$ cm^{-1}, $D_1 = 0.000$ cm^{-1}, $D_2 = 1.190$ cm^{-1}, $g = 2.092$, $zJ = 0.000$ cm^{-1}, and $R = 3.546 \times 10^{-4}$ (R is the least reliability factor). The positive values of J_1 and J_2 (0.367 cm^{-1} and 0.431 cm^{-1}) indicate the dominance of weak ferromagnetic coupling interactions of Gd···Gd and Gd···Cr in **1**, which are consistent with the experimental results.

Based on the large spin ground state value and negative magnetic anisotropy of compound **1**, the field-dependent magnetization was measured in the temperature range of 2.0–10.0 K and in the magnetic field range of 0–7 T (Fig. 5a). According to the Maxwell equation $\Delta S_m(T)\Delta H = \int[\partial M(T,H)/\partial T]_H dH$,[54] compound **1** showed the maximal $-\Delta S_m$ value of 21.1 J kg^{-1} K^{-1} at 5 K, 7 T (Fig. 5b), which was obviously lower than the estimated value of 37.57 J kg^{-1} K^{-1} (calculated by equation $-\Delta S_m = nR\ln(2S+1)$), which can be attributed to the small magnetic density induced by the large organic ligand L^- in compound **1**. Meanwhile, the

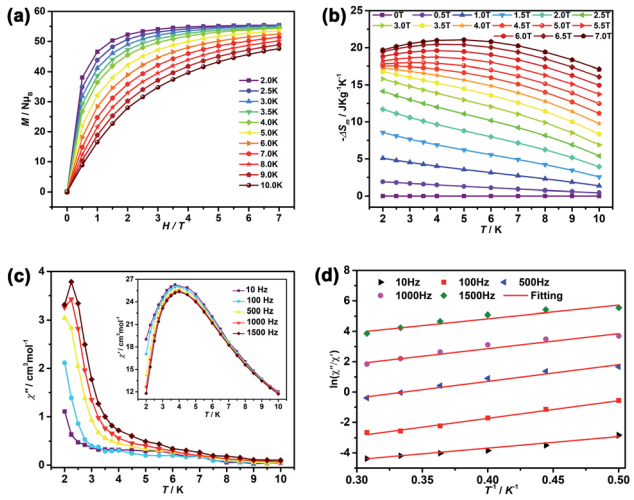

Fig. 5 (a) Magnetization for **1** in the temperature range of 2 and 10 K and the magnetic field range of 0–7 T. (b) $-\Delta S_m$ obtained from magnetization data of **1**. (c) Frequency dependence of χ'' and χ' (insert) with $H_{dc} = 2000$ Oe. (d) Results calculated by the simplified Debye function in the temperature range of 2.0–3.0 K.

temperature dependence of ac magnetic susceptibility was measured for **2** with $H_{dc} = 2000$ Oe at a different frequency. As shown Fig. 5c, frequency-dependent signals were observed before 10 K, implying slow relaxation of magnetization. However, no obvious peaks were observed because of quantum tunneling of magnetization (QTM).[55,56] The relaxation time and energy barrier could be obtained by the simplified Debye function $\ln(\chi''/\chi') = \ln(2\pi f\tau_0) + U/kT$.[57,58] Their values were shown as $\tau_0 = 3.98 \times 10^{-6}$ s and $U_{eff} = 1.15$ K, which are close to the anticipated characteristic energy gaps of 10^{-5}–10^{-12} s for Dy-containing cluster-based SMMs.[59,60]

4. Conclusions

In summary, two decanuclear Ln–Cr clusters of $\mathbf{Ln_7Cr_3}$ were prepared based on 2-pyrazinecarboxylic acid and acetate as mixed protecting ligands. Structure analysis showed that two trigonal bipyramids $\{Ln_3Cr_2\}$ formed the metal core of $\{Ln_6Cr_3\}$ as building blocks by sharing a common vertex of Cr^{3+} ion. Moreover, compound $\mathbf{Ln_7Cr_3}$ could form the three-dimensional framework with one-dimensional nanopore channel along the *a*-axis through the hydrogen-bond interaction between the cationic cluster core and the free mononuclear cation of $[Ln(H_2O)_8]^{3+}$ and the π-bond interaction between the pyrazine groups on the two cationic cluster cores. Magnetic experiment and calculation results indicated the dominance of weak ferromagnetic coupling interaction of Gd···Gd and Gd···Cr in **1**. Meanwhile, compound **1** showed the maximal $-\Delta S_m$ value of 21.1 J kg^{-1} K^{-1} at 5 K, 7 T, and compound **2** displayed obvious frequency-dependency but no obvious peaks due to QTM. Related work is ongoing by this group.

Conflicts of interest

There are no conflicts to declare.

Acknowledgements

The financial support for this work includes the National Natural Science Foundation of China (Grant No. 21802010, 21901002, 22022108) and the Natural Science Foundation of Anhui Province (Grant No. 1908085QB44) as well as the Open Project of the State Key Laboratory of Physical Chemistry of the Solid Surface of Xiamen University (Grant No. 201822).

Notes and references

1 X.-J. Kong, Y.-P. Ren, L.-S. Long, Z. Zheng, R.-B. Huang and L.-S. Zheng, *J. Am. Chem. Soc.*, 2007, **129**, 7016–7017.
2 X. J. Kong, Y. P. Ren, W. X. Chen, L. S. Long, Z. Zheng, R. B. Huang and L. S. Zheng, *Angew. Chem., Int. Ed.*, 2008, **47**, 2398–2401.
3 X. J. Kong, L. S. Long, R. B. Huang, L. S. Zheng, T. D. Harris and Z. P. Zheng, *Chem. Commun.*, 2009, 4354–4356.
4 X.-J. Kong, L.-S. Long, Z. Zheng, R.-B. Huang and L.-S. Zheng, *Acc. Chem. Res.*, 2009, **43**, 201–209.
5 X. Yang, D. Schipper, R. A. Jones, L. A. Lytwak, B. J. Holliday and S. Huang, *J. Am. Chem. Soc.*, 2013, **135**, 8468–8471.
6 Y. Xing, L. Q. Chen, Y. R. Zhao, X. Y. Zheng, Y. J. Zhang, X. J. Kong, L. S. Long and L. S. Zheng, *Inorg. Chem.*, 2019, **58**, 8494–8499.
7 J. B. Peng, Q. C. Zhang, X. J. Kong, Y. P. Ren, L. S. Long, R. B. Huang, L. S. Zheng and Z. Zheng, *Angew. Chem., Int. Ed.*, 2011, **50**, 10649–10652.
8 J. B. Peng, Q. C. Zhang, X. J. Kong, Y. Z. Zheng, Y. P. Ren, L. S. Long, R. B. Huang, L. S. Zheng and Z. Zheng, *J. Am. Chem. Soc.*, 2012, **134**, 3314–3317.
9 W. P. Chen, P. Q. Liao, Y. Yu, Z. Zheng, X. M. Chen and Y. Z. Zheng, *Angew. Chem., Int. Ed.*, 2016, **55**, 9375–9379.
10 W. P. Chen, J. Singleton, L. Qin, A. Camon, L. Engelhardt, F. Luis, R. E. P. Winpenny and Y. Z. Zheng, *Nat. Commun.*, 2018, **9**, 2107–2112.
11 D. P. Liu, X. P. Lin, H. Zhang, X. Y. Zheng, G. L. Zhuang, X. J. Kong, L. S. Long and L. S. Zheng, *Angew. Chem., Int. Ed.*, 2016, **55**, 4532–4536.
12 R. Chen, Z. H. Yan, X. J. Kong, L. S. Long and L. S. Zheng, *Angew. Chem., Int. Ed.*, 2018, **57**, 16796–16800.
13 W.-P. Chen, P.-Q. Liao, P.-B. Jin, L. Zhang, B.-K. Ling, S.-C. Wang, Y.-T. Chan, X.-M. Chen and Y.-Z. Zheng, *J. Am. Chem. Soc.*, 2020, **142**, 4663–4670.
14 R. Chen, G.-L. Zhuang, Z.-Y. Wang, Y.-J. Gao, Z. Li, C. Wang, Y. Zhou, M.-H. Du, S. Zeng, L.-S. Long, X.-J. Kong and L.-S. Zheng, *Natl. Sci. Rev.*, 2020, nwaa234.
15 R. Chen, C.-L. Chen, M.-H. Du, X. Wang, C. Wang, L.-S. Long, X.-J. Kong and L.-S. Zheng, *Chem. Commun.*, 2021, **57**, 3611–3614.
16 H. Zheng, M.-H. Du, S.-C. Lin, Z.-C. Tang, X.-J. Kong, L.-S. Long and L.-S. Zheng, *Angew. Chem., Int. Ed.*, 2018, **57**, 10976–10979.
17 X.-Y. Zheng, M.-H. Du, M. Amiri, M. Nyman, Q. Liu, T. Liu, X.-J. Kong, L.-S. Long and L.-S. Zheng, *Chem.–Eur. J.*, 2020, **26**, 1388–1395.

18 M.-H. Du, X.-Y. Zheng, X.-J. Kong, L.-S. Long and L.-S. Zheng, *Matter*, 2020, **3**, 1–16.
19 X. Y. Zheng, M. T. Chen, M. H. Du, R. J. Wei, X. J. Kong, L. S. Long and L. S. Zheng, *Chem.–Eur. J.*, 2020, **26**, 11985–11988.
20 X.-Y. Zheng, X.-J. Kong and L.-S. Long, in *Recent Development in Clusters of Rare Earths and Actinides: Chemistry and Materials*, ed. Z. Zheng, Springer Berlin Heidelberg, Berlin, Heidelberg, 2017, pp. 51–96.
21 S. Schmitz, J. van Leusen, N. V. Izarova, Y. Lan, W. Wernsdorfer, P. Kögerler and K. Y. Monakhov, *Dalton Trans.*, 2016, **45**, 16148–16152.
22 L. Qin, J. Singleton, W. P. Chen, H. Nojiri, L. Engelhardt, R. E. P. Winpenny and Y. Z. Zheng, *Angew. Chem., Int. Ed.*, 2017, **56**, 16571–16574.
23 Y.-M. Han, N.-F. Li, Y.-Z. Yu, J.-P. Cao, M.-X. Yang, Y.-L. Hong, R.-K. Kang, P. Yuan and Y. Xu, *RSC Adv.*, 2020, **10**, 11365–11370.
24 Y.-N. Gu, H. Yu, L.-D. Lin, Y.-L. Wu, Z. Li, W.-Y. Pan, J. He, L. Chen, Q. Li and X.-X. Li, *New J. Chem.*, 2019, **43**, 3011–3016.
25 S. Chen, V. Mereacre, Z. Zhao, W. Zhang, M. Zhang and Z. He, *Dalton Trans.*, 2018, **47**, 7456–7462.
26 Z. Fu, L. Qin, K. Sun, L. Hao, Y.-Z. Zheng, W. Lohstroh, G. Günther, M. Russina, Y. Liu, Y. Xiao, W. Jin and D. Chen, *npj Quantum Mater.*, 2020, **5**, 32–37.
27 J. J. Yin, C. Chen, G. L. Zhuang, J. Zheng, X. Y. Zheng and X. J. Kong, *Inorg. Chem.*, 2020, **59**, 1959–1966.
28 L. Qin, H.-L. Zhang, Y.-Q. Zhai, H. Nojiri, C. Schröder and Y.-Z. Zheng, *iScience*, 2021, **24**, 102350.
29 J. Rinck, G. Novitchi, W. Van den Heuvel, L. Ungur, Y. Lan, W. Wernsdorfer, C. E. Anson, L. F. Chibotaru and A. K. Powell, *Angew. Chem., Int. Ed.*, 2010, **49**, 7583–7587.
30 X.-Q. Wang, Z.-Y. Li, Z.-X. Zhu, J. Zhu, S.-Q. Liu, J. Ni and J.-J. Zhang, *Eur. J. Inorg. Chem.*, 2013, **2013**, 5153–5160.
31 K. R. Vignesh, S. K. Langley, A. Swain, B. Moubaraki, M. Damjanović, W. Wernsdorfer, G. Rajaraman and K. S. Murray, *Angew. Chem., Int. Ed.*, 2018, **57**, 779–784.
32 S. K. Langley, D. P. Wielechowski, V. Vieru, N. F. Chilton, B. Moubaraki, B. F. Abrahams, L. F. Chibotaru and K. S. Murray, *Angew. Chem., Int. Ed.*, 2013, **52**, 12014–12019.
33 Y. Yu, X. Pan, C. Cui, X. Luo, N. Li, H. Mei and Y. Xu, *Inorg. Chem.*, 2020, **59**, 5593–5599.
34 J.-J. Yin, T.-Q. Lu, C. Chen, G.-L. Zhuang, J. Zheng, X.-Y. Zheng and F. Shao, *Cryst. Growth Des.*, 2020, **20**, 4005–4012.
35 Z.-Y. Li, J.-J. Zhang, S.-Q. Liu, H. Zhang, Y.-J. Sun, X.-Y. Liu and B. Zhai, *Cryst. Growth Des.*, 2018, **18**, 7335–7342.
36 C. Cui, J. P. Cao, X. M. Luo, Q. F. Lin and Y. Xu, *Chem.–Eur. J.*, 2018, **24**, 15295–15302.
37 J.-L. Liu, Y.-C. Chen, F.-S. Guo and M.-L. Tong, *Coord. Chem. Rev.*, 2014, **281**, 26–49.
38 Z. Zheng, *Chem. Commun.*, 2001, 2521–2529.
39 X. Y. Zheng, X. J. Kong, Z. Zheng, L. S. Long and L. S. Zheng, *Acc. Chem. Res.*, 2018, **51**, 517–525.
40 O. V. Dolomanov, L. J. Bourhis, R. J. Gildea, J. A. K. Howard and H. Puschmann, *J. Appl. Crystallogr.*, 2009, **42**, 339–341.
41 M. Fugel, D. Jayatilaka, E. Hupf, J. Overgaard, V. R. Hathwar, P. Macchi, M. J. Turner, J. A. K. Howard, O. V. Dolomanov, H. Puschmann, B. B. Iversen, H.-B. Bürgi and S. Grabowsky, *IUCrJ*, 2018, **5**, 32–44.
42 G. M. Sheldrick, *Acta Crystallogr., Sect. A: Found. Adv.*, 2015, **71**, 3–8.
43 G. M. Sheldrick, *Acta Crystallogr., Sect. C: Struct. Chem.*, 2015, **71**, 3–8.
44 A. Spek, *Acta Crystallogr., Sect. C: Struct. Chem.*, 2015, **71**, 9–18.
45 L. Cao, T. Wang and C. Wang, *Chin. J. Chem.*, 2018, **36**, 754–764.
46 X.-Y. Zheng, J. Xie, X.-J. Kong, L.-S. Long and L.-S. Zheng, *Coord. Chem. Rev.*, 2019, **378**, 222–236.
47 H.-J. Lun, X.-J. Kong, L.-S. Long and L.-S. Zheng, *Dalton Trans.*, 2020, **49**, 2421–2425.
48 S. K. Langley, L. Ungur, N. F. Chilton, B. Moubaraki, L. F. Chibotaru and K. S. Murray, *Chem.–Eur. J.*, 2011, **17**, 9209–9218.
49 S. K. Langley, N. F. Chilton, B. Moubaraki, T. Hooper, E. K. Brechin, M. Evangelisti and K. S. Murray, *Chem. Sci.*, 2011, **2**, 1166–1169.
50 A. W. Addison, T. N. Rao, J. Reedijk, J. van Rijn and G. C. Verschoor, *J. Chem. Soc., Dalton Trans.*, 1984, 1349–1356.
51 A. Ruiz-Martinez, D. Casanova and S. Alvarez, *Chem.–Eur. J.*, 2008, **14**, 1291–1303.
52 D. Casanova, M. Llunell, P. Alemany and S. Alvarez, *Chem.–Eur. J.*, 2005, **11**, 1479–1494.
53 M. Pinsky and D. Avnir, *Inorg. Chem.*, 1998, **37**, 5575–5582.
54 M. Evangelisti and E. K. Brechin, *Dalton Trans.*, 2010, **39**, 4672–4676.
55 V. S. Parmar, F. Ortu, X. Ma, N. F. Chilton, R. Clerac, D. P. Mills and R. E. P. Winpenny, *Chem.–Eur. J.*, 2020, **26**, 7774–7778.
56 Y. S. Ding, K. X. Yu, D. Reta, F. Ortu, R. E. P. Winpenny, Y. Z. Zheng and N. F. Chilton, *Nat. Commun.*, 2018, **9**, 3134–3143.
57 D. Reta and N. F. Chilton, *Phys. Chem. Chem. Phys.*, 2019, **21**, 23567–23575.
58 K. S. Cole and R. H. Cole, *J. Chem. Phys.*, 1941, **9**, 341–351.
59 J. Cai, R. Ye, X. Liu, L. Guo and X. Qiao, *Dalton Trans.*, 2020, **49**, 16954–16961.
60 K. Zhang, V. Montigaud, O. Cador, G.-P. Li, B. Le Guennic, J.-K. Tang and Y.-Y. Wang, *Inorg. Chem.*, 2018, **57**, 8550–8557.